
Hydrothermal equilibria and ore formation

Alekhin Yu.V., Fiaizullina R.V., Bychkov D.A. Supramolecular geochemistry of real forms transfer in the gas-phase of heterophase fluids and composition of gas hydrate of mercury in the process of its local exhaustion in frozen

M.V. Lomonosov Moscow State University, Department of Geology, Moscow alekhin@geol.msu.ru

Abstract. Experimental studies of the solubility of low volatile compounds in the vapor aqueous phase directly indicate the degree of association of the solvent molecules themselves, that is, the variable fraction of associates of water vapor molecules depending on the $P-T$ parameters. A physico-chemical apparatus has been developed for analyzing such phenomena on a strict quantitative basis. The development of this idea allows you to create a basis for the supramolecular chemistry of a little dense aqueous gas solutions, since the version has been fully confirmed that the solubility of a nonvolatile chemical compound in a pair is a good witness to the degree of association of the water vapor itself as a solvent. This allows you to detail the actual stoichiometry of gas-vapor equilibria as complex formation reactions with a stable cluster $(H_2O)_4$, that is, a tetrahedron of water molecules that are actually responsible for the hydration and transfer of molecular addition complexes difficult to volatile compounds. Conscious re-standardization of the properties of water vapor, a direct account of the mole fraction of the real «active chemical principle», is a good example of studying changes in the solubility of volatile ingredients in the gas phase with the involvement of the ideas of gas dynamics.

Keywords: *volatile compounds, joining complexes, mercury gas hydrate, water vapor, water structure.*

Structural changes in water during its stabilization under the action of non-electrolyte molecules are interpreted differently. If we proceed from the two-structure model of water according to O.Ya. Samoilov, it should be assumed that its stabilization occurs as a result of partial filling of the tetrahedral structure of water with non-electrolyte molecules, displacing H_2O molecules from these voids that got into them during ice melting and the water temperature rises. This leads to an increase in the number of molecules with hydrogen bonds and tetrahedral coordination, on the one hand, and to the compaction of the structure of the solution at the expense of non-electrolyte molecules - on the other. The geometric similarity of ice Ih and water forms the basis of the O.A. Samoilov, explaining the anomalies of the properties of water by the progressive filling of the voids of the tetrahedral structure of ice with molecules of a collapsing and, at the same time, increasingly distorted framework, with increasing temperature. Pauling suggested that water has a clathrate structure observed in gas hydrates. In this model, the central molecule is

surrounded by a skeleton of water molecules forming pentagonal dodecahedrons. G.G. Malenkov and O.A. Samoilov showed that ice-like and clathrate structures are energetically close, but the former are more preferable at low temperatures. The possibility of the transition of a tetrahedral ice-like framework to dodecahedral structures of the clathrate type is not excluded, which can be associated with anomalies at 30-60°C that manifest themselves in the properties of water at 30-40°C. For our analysis, the cluster model of Frank and Wien (later developed by Namet and Sheraga) was of particular interest, which does not provide for a specific quasicrystalline structure, but only arbitrary formations of water molecules connected by hydrogen bonds (flickering clusters). According to our data in water vapor, the stabilization of water tetrahedra as the dominant tetrahedral structure (Alekhin, Vakulenko, 1987, Alekhin et al., 1994) is realized by the formation of $NaCl \bullet (H_2O)_4$ ¹ type addition complexes with different composition of the gas complex core. The water association constant for this equilibrium $4H_2O \leftrightarrow (H_2O)_4$ with stabilization of the tetrahedral structure in water vapor is shown in Figure 1. It is significant that for all such nonspecific stabilization reactions — attachment $\lg K_f = 0$ at the critical point of water. A similar approach was developed by us in the analysis of mercury gas complexes. Until recently, two problems remained unresolved in the atmospheric level of the mercury cycle of the mercury: 1) the mechanism of rapid leaching of mercury by rain after prolonged accumulation during periods of dry sunny weather; 2) a radical decrease in the total mercury content, up to its exhaustion, in periods when daily temperature fluctuations steadily vary around 0° C. The nature of the first phenomenon (rain washout) is related to the hydration of mercury oxide vapors: $HgO(g)$ and $Hg_2O_2(g)$. Previously, we experimentally showed that simple atomic mercury pairs are not hydrated (Alekhin, Fiaizullina, 2015). Low thermodynamic stability, rapid decomposition of solid mercury hydroxides do not prevent the accumulation of the corresponding hydroxo complexes: $Hg(OH)_2(aq)$, $Hg_2(OH)_2(aq)$. In the aqueous phase, they are quite stable. The subsequent leaching of these forms from the atmosphere is most effective in the form of microdroplets of water. This phenomenon determines all local and short-period variations in the content of mercury forms in the atmosphere.

¹ ● - with this sign, we show the supramolecular type of the joining (addition) complex.

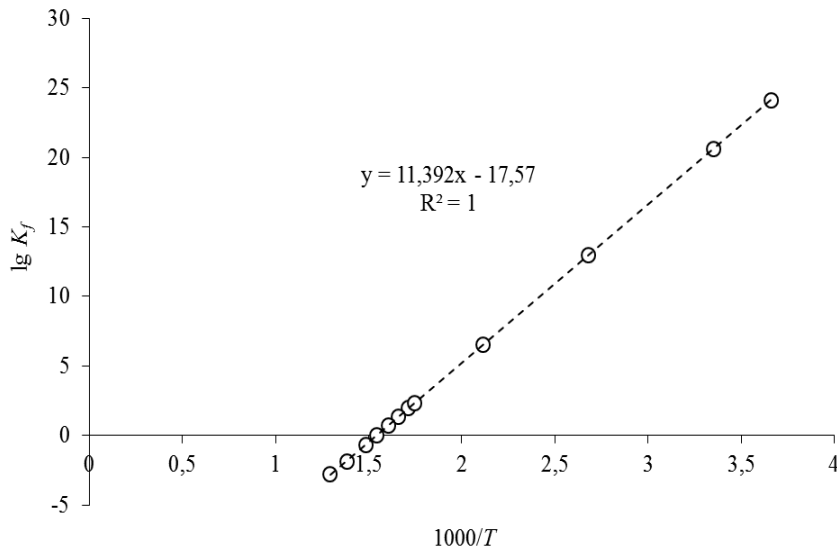


Fig. 1. Water association constant for gas equilibrium $4 \text{H}_2\text{O} \leftrightarrow (\text{H}_2\text{O})_4$

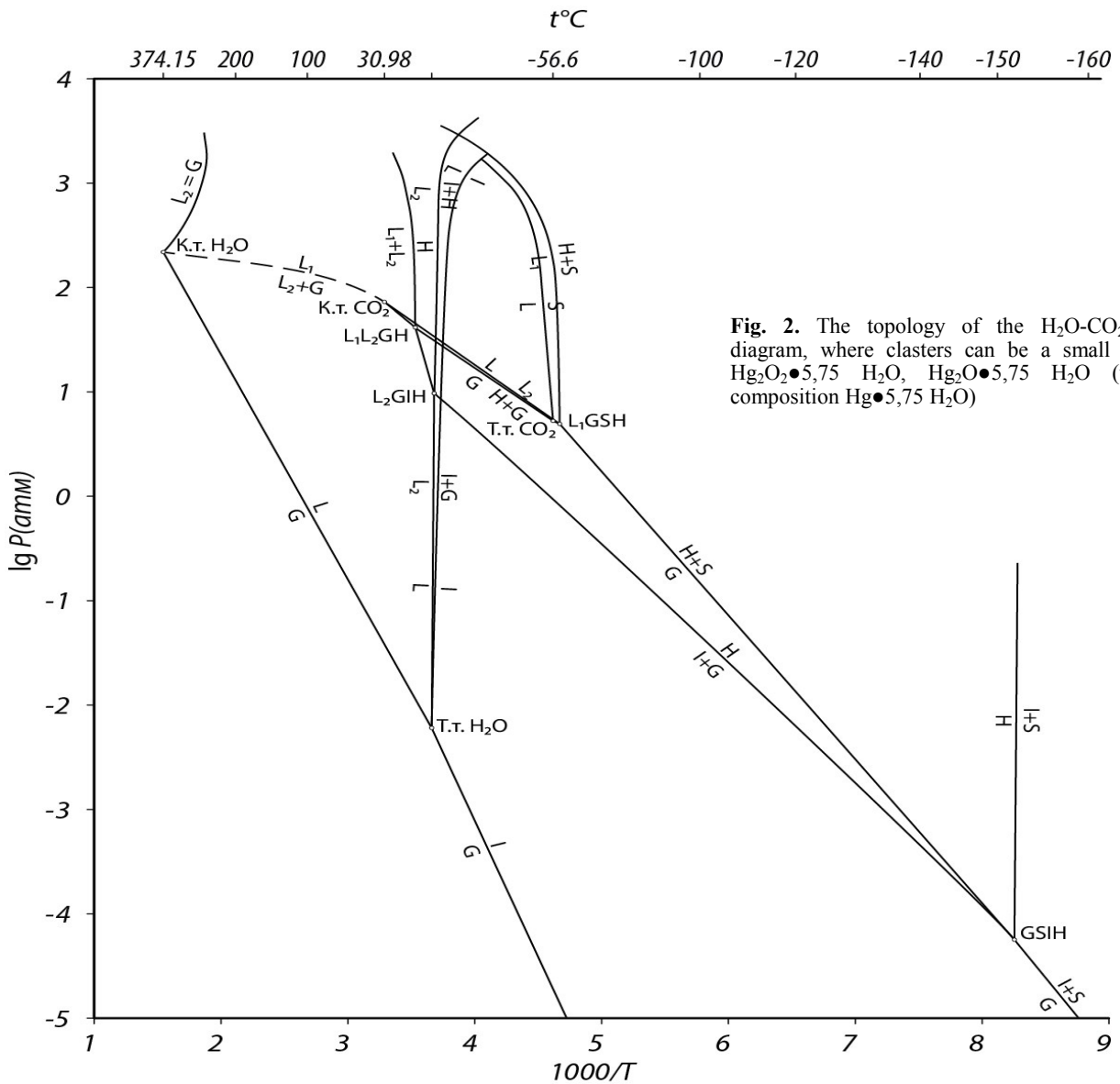


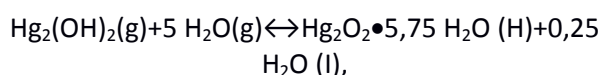
Fig. 2. The topology of the $\text{H}_2\text{O}-\text{CO}_2$ phase diagram, where clusters can be a small «guest» $\text{Hg}_2\text{O}_2 \bullet 5,75 \text{H}_2\text{O}$, $\text{Hg}_2\text{O} \bullet 5,75 \text{H}_2\text{O}$ (unlikely composition $\text{Hg} \bullet 5,75 \text{H}_2\text{O}$)

Until recently, the second mechanism remained quite mysterious and more interesting. It controls the maintenance of a practically stable (but not conservative) atmospheric level of global mercury

content of 2.2 ng/m^3 (as a stable average). Our monitoring of daily variations in mercury concentrations (during periods when the mean daily temperature fluctuates around the triple point of

water) showed that daily (and completely reversible) mercury exhaustion occurs. This phase transition was initially interpreted by us as the reaction of formation of gas hydrate (H) from mercury vapor Hg(0) according to a simple scheme: $\text{Hg(g)} + 5.75 \text{ H}_2\text{O(g)} = \text{H}$, where $\text{H} = \text{Hg} \bullet 5.75 \text{ H}_2\text{O}$. However, it was clear that the formation of a clathrate solid solution of implantation may be more complex and accompanied by oxygen pressure of 0.208 atm not only changes in the structure of ice water ($\text{I}_h \rightarrow \text{H}$), but also changes in the valence of mercury in the structure of phase H according to the schemes: $\text{Hg} + 0.5 \text{ O}_2 = \text{HgO}$ and redox disproportionation: $2\text{HgO(II)} = \text{Hg}_2\text{O(I)} + \text{Hg(0)}$. According to our data (Alekhin et al., 1973), a topological analysis of the stability of gas hydrates in water – gas systems $\text{H}_2\text{O} - \text{CO}_2$ (Fig. 2) and $\text{H}_2\text{O} - \text{H}_2\text{S}$ (Alekhin, Sretenskaya, 1983) showed that the temperature of the inevitable complete decomposition of such solid. The solutions are close to 121 K (-150°C) and 126 K (-147°C), respectively, and controlled by partial pressures over the “guests” molecules (CO_2 , H_2S) and the vapor pressure of the water over ice as the «host». Estimation of the lower stability temperature of the analogous, gas hydrate $\text{Hg} \bullet 5.75 \text{ H}_2\text{O}$ without experimental data is difficult, but is possible. If we assume, after (Schuster et al., 2002), that the cause of the global accumulation (and sustainable conservation) of mercury in a concentration of 4 ppt in permafrost, (in the form of a gas hydrate), which in our version is due to its stability with known Hg(0) volatility, which corresponds to an air content of 2.2 ng/m^3 , that is, at a partial pressure of $\text{Hg} = 2.46 \cdot 10^{-13}$ and compare this value with the content of mercury (4 ppt $\sim X = 3.6 \cdot 10^{-13}$ in permafrost ice, it is easy to calculate the typical composition of a gas hydrate as $\text{Hg} \bullet 6.05 \text{ H}_2\text{O}$ (H), slightly different from the theoretical, to which corresponds to the filling of structural cavities in gas hydrates of the corresponding structural type. The analogy with the $\text{H}_2\text{O} - \text{CO}_2$ system and the polar caps of Mars are not accidental (Alekhin et al., 1977).

There are deep analogies between the migration of carbon dioxide and the formation of its gas hydrate on the polar caps of Mars, and a similar freezing process, which controls a stable level of mercury in the Earth’s atmosphere during accumulation, conservation in ice sheets and in the permafrost. A more detailed analysis of the most acceptable candidate for the stable existence of a mercury gas hydrate impurity showed that it is mercury oxide, Hg(I) is a hydrated metallocycle $\text{Hg}_2\text{O}_2 \bullet 5.75 \text{ H}_2\text{O}$, the formation of which corresponds to the scheme:



what happens during freezing. The stoichiometry of this reaction corresponds exactly to the steady

accumulation of mercury in the background (4 ppt) in the ice, which closes the discussion about the actual composition and stoichiometry of mercury gas hydrate. However, this simple scheme does not directly take into account the fact that the Hg_2O_2 mineral is only an admixture, a «minor guest» of the structure of the main gas hydrate: carbon dioxide. In the gas phase, the possibility of domination of the addition complex: $\text{Hg}_2(\text{OH})_2 \bullet (\text{H}_2\text{O})_4(\text{g})$, stabilized by its «mercury nucleus», $\text{Hg}_2(\text{OH})_2$, was discussed by us earlier (Alekhin et al., 2018).

In this case, we also use the previously formed synthetic function $F = -\lg(\varphi_2/X_2)_T = \lg(X_2^2 P/f_2^\circ)_T$ at $P \rightarrow p_2^\circ \sim 0$ for the volatile substances $F \rightarrow 0$, when $\varphi_2 \rightarrow 1$ and $X_2 \rightarrow 1$. Thus, laying on the axes $y=F$, $x=P$, we get a family of lines coming to the origin if the volatility of the edge component f_2° is chosen correctly. Thus, the analysis of experimental data on the solubility of KCl in water vapor using this function revealed three temperature regions of the predominance of various complex forms of KCl hydrates in the gas phase:

1. KCl monomer $\text{KCl} \bullet (\text{H}_2\text{O})_4$ is the predominant form of the dissolved edge component at 250–300 °C (and, obviously, lower in temperature).

2. Dimer $\text{K}_2\text{Cl}_2 \bullet (\text{H}_2\text{O})_4$ dominates at 350 °C and in the region of sufficiently high pressures (the region of stoichiometric four-hydrate predominance) on the isotherm of 400 °C.

3. Trimer $\text{K}_3\text{Cl}_3 \bullet (\text{H}_2\text{O})_4$ dominates on the isotherms of 450–500 °C in the entire range of studied pressures and at sufficiently low pressures on the isotherm of 400 °C.

The linearity of the function $\lg F = \lg(PX_2^2/f^\circ)$ KCl, K_2Cl_2 , K_3Cl_3 and NaCl, Na_2Cl_2 is performed with the correct choice of the volatility of the dominant associate in the nucleus of the addition complex.

CONCLUSIONS

1. For dense water, the most realistic model of «flickering clusters» reconciles all the ideas, starting from the works of Fowler – Guggenheim, Pauling and the later works of Samoilov – Malenkov. However, according to our experimental data for the low-density aqueous phase, i.e. for the S – G equilibrium when dissolving non-volatile compounds, the specificity of the interaction and the dissolution of salts is accompanied by additional stabilization of water tetrahedra $(\text{H}_2\text{O})_4$ as the dominant of the tetrahedral structure in water vapor: $\text{NaCl} \bullet (\text{H}_2\text{O})_4$, $\text{Na}_2\text{Cl}_2 \bullet (\text{H}_2\text{O})_4$ and for KCl: $\text{KCl} \bullet (\text{H}_2\text{O})_4$, $\text{K}_2\text{Cl}_2 \bullet (\text{H}_2\text{O})_4$, $\text{K}_3\text{Cl}_3 \bullet (\text{H}_2\text{O})_4$ with integer stoichiometry, in the spirit of the ideas of the molecular dynamics of real particles (Len, 1998). We extend this approach to forms of mercury in the vapor phase.

2. For the temperature range of 25–100 °C, the Henry’s constant values for the heterophase reaction

Hydrothermal equilibria and ore formation

$\text{Hg}_{(\text{liq})} \leftrightarrow \text{Hg}_{(\text{aq})}$ were experimentally found, which allow us to recommend the following values for the equilibrium of mercury vapors with an aqueous solution: $\lg K_H = -2.41$ at 25 °C and $\lg K_H = -2.43$ at 100 °C (Alekhin et al., 2011). The results of estimation let the Henry's constants made it possible to detect a distinct but small extremum at temperatures of 120–130 °C, close to the position of extremes in systems with inert gases (Ar, Kr).

3. The exchange of mercury between geochemical reservoirs is regularly reflected in cyclical daily and seasonal variations in atmospheric concentrations of 0.2–25 ng/m³ with a steady average of 2.2 ng/m³ for background areas (more than 100 thousand measurements). Simultaneous measurements of regional variations in the densities of these flows provide important information on the local intensity of mercury exchange processes in geochemical reservoirs.

4. With a modern content in the atmosphere of CO₂ (410 ppm, $X(\text{CO}_2)/X(\text{H}_2\text{O}) = 0.154$ at $X(\text{Hg}_2\text{O}_2)/X(\text{H}_2\text{O}) = 1.23 \cdot 10^{-13}$, that when the content in permafrost 4 ppt of mercury corresponds to the formation of phase H, gas hydrate $\text{CO}_2 \bullet 5.75 \text{H}_2\text{O}$, but with a small admixture of $\text{Hg}_2\text{O}_2 \bullet 5.75 \text{H}_2\text{O}$, as a tracer in an amount corresponding to the ratio $X(\text{Hg}_2\text{O}_2)/X(\text{H}_2\text{O}) = 1.23 \cdot 10^{-13}$.

5. Our monitoring of daily variations in mercury content (during periods when the average daily temperature fluctuates around the triple point of water) showed that daily (and completely reversible) exhaustion of mercury occurs. We interpreted this phase transition as the reaction of gas hydrate (H) formation from the metallocycle (Hg–O–O–Hg) of monovalent mercury Hg(I) according to the scheme: $\text{Hg}_2\text{O}_2(\text{g}) + 5.75 \text{H}_2\text{O}(\text{g}) = \text{Hg}_2\text{O}_2 \bullet 5.75 \text{H}_2\text{O}$. It cannot be ruled out that sublimation (or disintegration of the clathrate solid interstitial solution) is accompanied by both a change in the structure of ice (I_h) and a change in the valence of mercury according to the schemes: $\text{Hg}_2\text{O}_2(\text{I}) = 2 \text{HgO}(\text{II})$ or redox disproportionation: $\text{Hg}_2\text{O}_2(\text{I}) = \text{Hg}_2\text{O}(\text{I}) + \text{Hg}(\text{0})$. According to the analysis of the stability of gas hydrates in the H₂O–CO₂ and H₂O–H₂S systems, the final decay temperatures of clathrate solid solutions are close to 121 K (–150 °C) and 126 (–147 °C) and controlled by the approach of saturated vapor pressures over the “main guests” (CO₂, H₂S and «small»: Hg₂O₂) and ice water as the «host». A reliable estimate of the lower stability temperature of $\text{Hg}_2\text{O}_2 \bullet 5.75 \text{H}_2\text{O}$ without experimental data is difficult, but, as a first approximation, it is possible. We believe that the accumulation (and complete preservation) of this clathrate (4 ppt) in permafrost is entirely related to the stability of carbon dioxide gas hydrate with the thermodynamic volatility of the Hg₂O₂ metallocycle, corresponding to its content of 2.2 ng/m³ at a partial

pressure of $\text{Hg} = 2.5 \cdot 10^{-15}$ and the mole fraction of $\text{Hg}_2\text{O}_2(\text{I}) = 2,2 \cdot 10^{-15}$ («small guest»).

This work was supported by RFBR grants №17-05-01055 and 19-05-00519.

References:

- Alekhin Yu.V., Vakulenko A.G. The solubility and thermodynamic properties of NaCl in water vapor at temperatures of 300–500 °C and pressures up to 300 bar. // *Geochemistry*, 1987. N. 10. P. 1468–1481. In Rus.
- Alekhin Yu.V., Vakulenko AG, Razina M.V. Solubility and molecular hydrolysis in low-density fluids // *Exp. problems of geology*. M.: Nauka, 1994. P. 543–555. In Rus.
- Alekhin Yu.V., Zharikov V.A., Zakirov I.V. System H₂O–CO₂ and the atmospheres of the planets // *Results of science and technology. Geochemistry. Mineralogy. Petrography*. Vol. 7. M.: VINITI, 1973. P. 5–78. In Rus.
- Alekhin Yu.V., Zagrtedov N.R., Mukhamadiyarova R.V. Hg⁰(liq) – Hg⁰(solution) equilibrium and solubility of elementary mercury in water // *Moscow Univ. Geol. Bul.*, 2011. Ser. 4: Geology. No. 6. P. 439–441.
- Alekhin Yu.V., Zakirov I.V., Bazilevsky A.T., Florensky K.P. Composition of polar caps of Mars. // *Geokhimiya*, 1977. N. 9. P. 1283–1287.
- Alekhin Yu.V., Sretenskaya N.G. System H₂O–H₂S // *Experimental studies of endogenous ore formation*. M.: Nauka, 1983. – 250 p. (P. 61–89). In Rus.
- Alekhin Yu.V., Fiaizullina R.V. The main valence mercury forms equilibria in the two-phase fluids // *Experimental Geochemistry*, 2015. Vol. 3. P. 30–36.
- Alekhin Yu.V., Fiaizullina R.V., Bychkov D.A. Topological analysis of phase equilibria in the Hg–H₂O system, thermodynamic properties of the main valence forms of mercury and their prevalence in nature // *Proceedings of the 3rd Scientific Conference «Geological evolution of water interaction with rocks» Ulan-Ude*, 2018. P. 248–252. In Rus.
- Len J.M. *Supramolecular Chemistry: Concepts and Prospects*. Novosibirsk: Nauka, 1998. – 334 p. In Rus.
- Schuster P.F., Krabbenhoft D.P. et al. Atmospheric mercury deposition during the last 270 years: a glacial ice core record of natural and anthropogenic sources // *Environ. Sci. Technol.*, 2002. Vol. 36. P. 2303–2310.

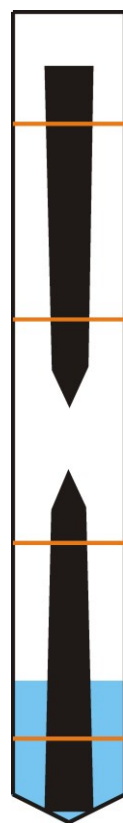
Alekseyev V.A., Burmistrov A.A., Gromiak I.N. Transformation of quartz into opal in closed water–vapor system

Vernadsky Institute of Geochemistry and Analytical Chemistry RAS, Moscow (alekseyev-v@geokhi.ru)

Abstract. Long-term experiments were performed at 300°C with quartz crystals, the lower parts of which were located in liquid water, and the upper parts in water vapor. After the experiments, the concentration of dissolved silica was significantly lower than the solubility of quartz. However, metastable opal was formed on the surface of stable quartz crystals above the water-vapor boundary. This unusual behavior of silica is explained by distillation initiated by the predominant evaporation of a thin film of water at contact with quartz. The process was intensified by wetting quartz with a thin film of water, which rose along the rough surface of the crystal above the water-vapor boundary and increased the evaporation area. Evaporation led to an increase in the concentration of silica, which was deposited on quartz in the form of opal. Mineral transformations during distillation occur far from equilibrium, so their rates are much higher compared to simple recrystallization caused by a small temperature gradient. The described phenomenon may be the cause of asymmetry of natural crystallization cavities, the lower parts of which were dissolved, and minerals were deposited in the upper parts.

Keywords: quartz, opal, transformation, water–vapor system

Introduction. Water-rock interaction is usually studied using thermodynamics and kinetics of chemical reactions, as well as transport processes: filtration, diffusion and heat transfer. Recently, there is a shift of these studies to the nanoscale, where new properties of particles and fluids are found (Alekseyev, 2019). The most interesting properties are those that radically change the behavior of macro systems. For example, the evaporation of a thin (<100 nm) layer of solution at contact with the wall of platinum ampoule led to the transformation of stable quartz into a metastable opal, which was deposited on the wall above the solution level (Alekseyev, Medvedeva, 2018). In this paper, we have tried to perform such a transformation in a more real for nature conditions, replacing the platinum wall by the quartz crystal itself. This can serve as convincing evidence that the observed phenomenon is not an exclusively experimental artifact.



Methods. Distilled water and natural crystals of α -quartz from Brazil (Minas Gerais state) were used in the experiments. Transparent and colorless crystals had the form of a hexagonal prism with a small conicity to the top of 6-7 cm long, ~10 mm in diameter and a mass of 6.4-8.6 g. The crystals were fixed with wire clamps (aludel) along the axis of the autoclave so that one crystal was located at the bottom and the other at the top (Fig. 1). The mass of water (6 g) was selected so that at the temperature of the experiment (300°C) only a part of the lower crystal (2.5 cm) was in water (filling coefficient was 0.15), and its upper part and the upper crystal were in water vapor. Two autoclaves, equipped in this way, were placed in a vertical electric furnace on

Fig. 1. Scheme of experiment

each other and heated at $300\pm 2^\circ\text{C}$ with different vertical temperature gradients (TG) on the surface of the lower and upper autoclave (Tab. 1). After 42 days, the autoclaves were quenched in cold water, the solutions were filtered (filter pore size was 0.05 microns) and analyzed (ICP AES). Silica concentrations in quenched solutions were recalculated to the temperature of the experiments taking into account the solution dilution by condensate during quenching (Verma, 2000). Newly formed silica was studied using endoscope, X-ray diffraction, optical and scanning electron microscope (SEM).

Results. Concentrations of dissolved silica in experiments m (Tab. 1) was noticeably lower than the solubility of quartz, which is close to 10 mmol/kg (Alekseyev et al., 2018). Weight loss of top crystals in both experiments was negligible, and for the bottom crystals it was bigger and exceeded the weight of the dissolved silica M_1 (Tab. 1).

Table 1. The conditions and results of experiments with quartz and water: the temperature gradient on the surface of the autoclave from the bottom up (TG), the concentration of dissolved silica at 300°C (m), the mass of dissolved silica (M_1), the mass of newly formed silica on the wall of the autoclave (M_2), mass loss crystals (ΔM).

Position of the autoclave	TG, %/cm	m , mmol/kg	M_1 , mg	M_2 , mg	ΔM of crystal, mg	
					Upper	Lower
Top	-0.08	8.2	3.0	9.0	-0.8	-24.4
Bottom	+0.15	6.2	2.2	9.0	-1.1	-18.3

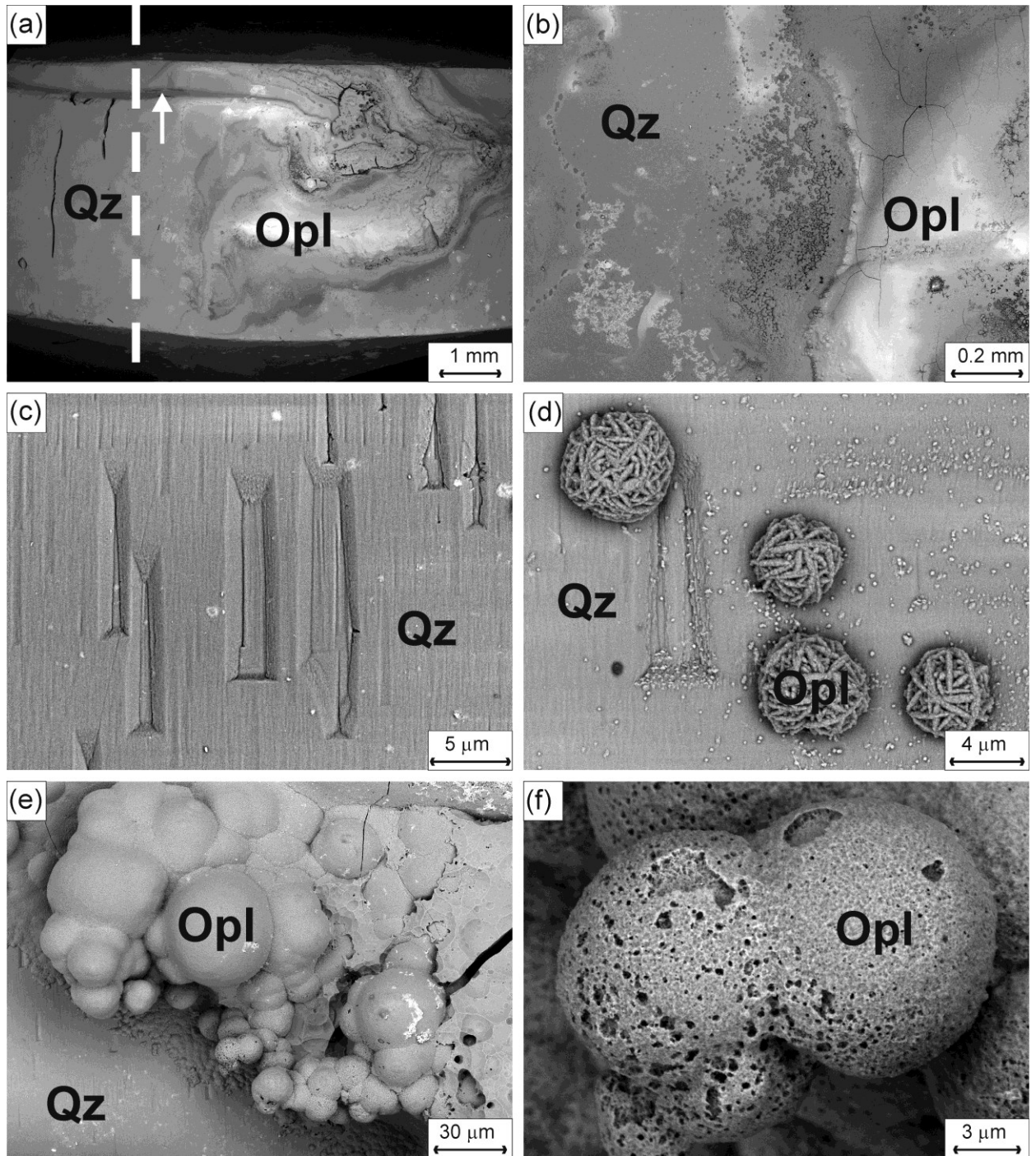


Fig. 2. SEM photo of opal (Opl), formed on quartz (Qz). (a) - a general view (the dotted line shows the level of the solution in the experiment, the arrow shows the groove along which the solution was raised); (b) - detail of the photo (a); (c) - etching pits on quartz; (d) - opal spheres composed of microcrystals; (e) - cluster-shaped opal; (f) - detail of the photo (d).

The newly formed silica was deposited on the inner walls of autoclaves in the form of white rings at the level of the water surface (M_2), as well as on the lower crystal in the lower autoclave. According to X-ray diffraction, this silica is similar to microcrystalline cristobalite-tridymite opal, which was found in our previous studies (Alekseyev, Medvedeva, 2018). On the quartz crystal, opal was deposited above the water level and, with a slight magnification, looked like an irregular shaped sinter aggregate (Fig. 2a and 2b). Numerous trough-shaped etching pits were observed on the quartz surface

below opal (Fig. 2c). In the transition zone between the quartz and the opal aggregate, separate opal spheres (Fig. 2b), composed of microcrystals (Fig. 2d), were observed. The bulk of the opal is composed of similar spheres, merged completely or partially into crusts (Fig. 2e and 2f).

Discussion. Opal is formed as a result of accumulation of silica skeletons of seaweed, microorganisms in the seas and by precipitation of silica from supersaturated solutions. In the latter case, the supersaturation is created by lowering the temperature, pH, evaporation of the solution or

dissolution of silicates. The formation of metastable opal in the field of stability of quartz is explained by the nucleation mechanism with the small size of its critical nucleus (Okamoto et al., 2010). First, noncrystalline opal-A (an analogue of amorphous silica) is formed, which slowly turns into microcrystalline opal (solid solution of tridymite and cristobalite) and then into quartz by the dissolution – crystallization mechanism (Williams, Crerar, 1985).

From the point of view of traditional geochemistry, the formation of opal in this system is possible only with a very large temperature difference between the top and bottom of the autoclave (~200°C). In this case, we can expect only the saturation of the solution with silica and the subsequent recrystallization of quartz, caused by the temperature gradient and the temperature dependence of the solubility of quartz. Let us estimate the rate of these two processes. The time of dissolution of quartz in water is described by the following equation (Rimstidt, Barnes, 1980):

$$t = - \left[\frac{1}{(k/m_{eq})(S/M)} \right] \ln \left(1 - \frac{m}{m_{eq}} \right), \quad (1)$$

where m and m_{eq} are the actual and equilibrium concentration of dissolved silica (mol / kg), S is the surface area of the mineral (m²), M is the solution mass (kg), k is the quartz dissolution rate constant (mol m⁻² s⁻¹). $S = 8.15 \times 10^{-4}$ m² (part of the crystal submerged in water), $M = 4.3 \times 10^{-3}$ kg (at 300°C). The values of k and m_{eq} are taken from (Tester et al., 1994) and (Rimstidt, Barnes, 1980), respectively. The values of S and k correspond to the geometric surface area calculated from the size and shape of the crystals (hexagonal prism). Such an approach better corresponds to the reaction mechanism of quartz dissolution, when the bottom of the etching pit is actively dissolved, and its side walls remain passive (Gautier et al., 2001). Calculations by equation (1) showed that the equilibrium ($m / m_{eq} = 0.9975$) should be achieved within 2 days.

During recrystallization, a steady state is established with equal rates of dissolution of quartz in water r_1 (left) and precipitation of quartz in vapor r_2 (right):

$$k_1 S_1 (1 - m/m_{eq1}) = -k_2 S_2 (1 - m/m_{eq2}) \quad (2)$$

where subscripts 1 and 2 refer to crystals located in water and vapor at temperatures of 300 and 299.44°C. This temperature difference corresponds to the experimental design (Fig. 1) and the direction of the TG, which is favorable for the rapid transfer of SiO₂ by convection of the solution under the action of buoyancy forces. $S_1 = 8.15 \times 10^{-4}$ m² (crystal area in water), $S_2 = 3.045 \times 10^{-3}$ m² (crystal area in vapor). The value of m / m_{eq} in vapor is the same as in water with an equilibrium distribution of dissolved silica between vapor and water (Plyasunov, 2012). The

value of m , calculated from equation (2), was substituted into the left or right side of this equation and the value of r_1 or r_2 was calculated. The calculations gave $r_1 = -r_2 = 3.81 \times 10^{-12}$ mol / s, which corresponds to 0.8 mg of SiO₂, redeposited in 40 days. This value is not only the maximum possible, but also greatly overestimated, since the k_2 value for vapor (it is unknown) must be significantly less than the k_2 value used for water. Nevertheless, the calculated value (0.8 mg) remains an order of magnitude less than the mass of silica deposited on the walls of autoclaves (Table 1). Thus, the traditional approach is not able to adequately predict either the phase composition of the real system, nor the rate of mineral transformations in it.

The formation of opal in this system means the existence of highly supersaturated solutions during the dissolution of quartz. This is possible if dissolution and precipitation occurs in solutions with different concentrations of silica. At quartz crystal and at an autoclave wall, which have a higher thermal conductivity than water, overheating of a thin water film occurs relative to the rest of water surface (Plawsky et al., 2008). A higher temperature of the film corresponds to a higher pressure of saturated water vapor than the pressure that exists in the autoclave. Therefore, evaporation on the water film somewhat predominates over condensation. On the remaining surface of the solution, condensation somewhat predominates over evaporation in order to reduce the excess pressure of water vapor created by evaporation of the water film to its equilibrium pressure with the volume of the solution. The hydrophilicity and surface roughness of quartz cause the solution film to rise from its main volume under the action of capillary forces (Friedman et al., 2013; Bico et al., 2002), which significantly increases the area of preferential evaporation. As a result, the solution is distilled (Alekseyev, Medvedeva, 2018). The proximity of the deposition of opal with a groove that intersected the water–vapor boundary (Fig. 2a) is hardly accidental. Most likely, the water rose along this groove into the vapor phase, spread over the surface of quartz and evaporated, depositing silica, the sintering form of which marked the paths of the solution.

With simultaneous processes of quartz dissolution and solution distillation, a steady state was also established but a constant m value can be significantly lower than the solubility of quartz (Alekseyev, Medvedeva, 2018). Calculation by equation (2) at $S = 8.15 \times 10^{-4}$ m² (submerged part of the lower crystal) and $m = 6.25 \times 10^{-3}$ mol/kg (table. 1) gave $r_1 = 5.1 \times 10^{-10}$ mol/s, which corresponds to the formation of 106 mg SiO₂ for 40 days. This value is 130 times greater than the maximum possible value for simple recrystallization of quartz (see above). Calculations using the model of distillation taking

Hydrothermal equilibria and ore formation

into account the dissolution of quartz (Alekseyev, Medvedeva, 2018) with the values accepted, gave a close value of r_1 and the distillation rate of 7.7 g/day, i.e. the entire solution in the autoclave passed through the vapor phase in less than a day. Thus, the distillation of the solution, caused by the abnormal properties of the nanofilm fluid and capillary forces, radically changes the phase composition of the system and the rate of mineral transformation.

For open natural systems, processes leading to results similar to the result of our research are known. For example, the creeping of a salt solution in the form of a thin film outside its main volume and the subsequent evaporation of the film causes the creeping of the salt itself (Van Enkevort, Los, 2013). The unusual transformation of quartz into opal was observed during the weathering of fossilized wood (microcrystalline quartz), which partially protruded from the slope of the river (Senkayi et al., 1985). Having a high porosity, it could play the role of a pump that sucked in ground water under the action of capillary forces and saturated the water with silica. This water rose to the surface and evaporated, causing the deposition of opal. As our research has shown, such phenomena are also possible for closed systems. For example, the often-observed asymmetry of crystallization cavities (large crystals at the top) under natural conditions (Askhabov, 1993) can be explained by the distillation of solution that partially fills the cavity. This cavity has the ability to migrate down due to the constant dissolution of its bottom. As a result, a small volume of the solution can cause phase transformations in a large volume of rock. These transformations are able to proceed from stable to metastable phases at a rate that is much higher than the rate of simple recrystallization.

References:

- Alekseyev V.A. Nanoparticles and nanofluids in water–rock interactions // *Geochem. Int.* 2019. Vol. 57. № 4. P. 357-368.
- Alekseyev V.A., Medvedeva L.S. Silica distribution in the system quartz–water–vapor depending on the temperature gradient // *Geochem. Int.* 2018. Vol. 56. № 2. P. 136-147.
- Ashabov A.M. Crystal genesis and evolution of “crystal–environment” system. Saint-Petersburg: Nauka, 1993. 154 p. (in Russian).
- Bico J., Thiele U., Quéré D. Wetting of textured surfaces // *Colloids and Surfaces A*. 2002. Vol. 206. P. 41-46.
- Friedman S.R., Khalil M., Taborek P. Wetting Transition in Water // *Phys. Rev. Lett.* 2013. Vol. 111. № 22. 226101.
- Gautier J.-M., Oelkers E.H., Schott J. Are quartz dissolution rates proportional to B.E.T. surface areas? // *Geochim. Cosmochim. Acta.* 2001. Vol. 65. № 7. P. 1059-1070.
- Okamoto A., Saishu H., Hirano N., Tsuchiya N. Mineralogical and textural variation of silica minerals in hydrothermal flow-through experiments:

Implications for quartz vein formation // *Geochim. Cosmochim. Acta.* 2010. Vol. 74. № 13. P. 3692-3706.

- Plawsky, J.L., Ojha, M., Chatterjee, A., Wayner Jr., P.C. Review of the effects of surface topography, surface chemistry, and fluid physics on evaporation at the contact line // *Chem. Engin. Commun.* 2008. Vol. 196. P. 658-696.
- Plyasunov A.V. Thermodynamics of Si(OH)₄ in the vapor phase of water: Henry’s and vapor–liquid distribution constants, fugacity and cross virial coefficients // *Geochim. Cosmochim. Acta.* 2012. Vol. 77. P. 215-231.
- Rimstidt J.D., Barnes H.L. The kinetics of silica–water reactions // *Geochim. Cosmochim. Acta.* 1980. Vol. 44. № 11. P. 1683-1699.
- Senkayi A.L., Dixon J.B., Hossner L.R., Yerima B.P.K., Wilding L.P. Replacement of quartz by opaline silica during weathering of petrified wood // *Clays and Clay Minerals.* 1985. Vol. 33. № 6. P. 525-531.
- Tester J.W., Worley W.G., Robinson B.A., et al. Correlating quartz dissolution kinetics in pure water from 25 to 625°C // *Geochim. Cosmochim. Acta.* 1994. Vol. 58. № 11. P. 2407-2420.
- Van Enkevort W.J.P., Los J.H. On the creeping of saturated salt solutions // *Cryst. Growth Des.* 2013. Vol. 13. № 5. P. 1838-1848.
- Verma M.P. Chemical thermodynamics of silica: a critique on its geothermometer // *Geothermics.* 2000. Vol. 29. P. 323-346.
- Williams L.A., Crerar D.A. Silica diagenesis, II. General mechanisms // *J. Sedimentary Petrology.* 1985. Vol. 55. № 3. P. 312-321.

Ermina O.S.¹, Bychkov A.Y.^{1,2} Hydrothermal transformation of biomass *Chlorella sp.* at different temperature. UDC 550.4.02

¹M.V. Lomonosov Moscow State University, Department of Geology, Russia, Moscow, ²V.I. Vernadsky Institute of Geochemistry and Analytical Chemistry RAS, Russia, Moscow. ermina6@yandex.ru, andrewbychkov@rambler.ru

Abstract. In recent years great emphasis is placed on the study of alternative energy sources. In our research experiments were performed with algae biomass *Chlorella sp.* in titanium autoclaves with a volume of 20 ml at temperatures of 250-350°C and pressure of saturated water vapor. The duration of the experiments was 3 and 7 days. The results showed that the mineral phases reduce the oil yield, but improve its quality. The largest oil yield is observed at temperatures of 250-300°C, and gas - at a temperature of 300°C. An increase in the duration of the experiments over contributes to an increase in the oil yield and a decrease in the gas yield.

Keywords: Bio-oil, Algae, *Chlorella Sp.*, Temperature, Mineral, Gas, Experiment.

Recently, much attention has been paid to the study of alternative energy sources. A lot of works have been devoted to the transformation of algae

biomass into hydrocarbons. The optimal temperature of hydrothermal treatment (Shakya et al., 2015; Biswas et al., 2017), effects of added catalysts (Anastakis, Ross, 2011; Shakya et al., 2015), increased oil output by risen heating rate (Bach et al., 2014) were studied, also oil production from different algae species and differences of output were investigated (Reddy et al., 2016) and the gas phase was studied (Fahmy et al., 2018; Yanika J. et al., 2013). In these papers the possibility to obtain a mixture of hydrocarbons similar in composition to natural heavy oil or bitumen and gas from algae biomass has been demonstrated. In this research organic composition of products was not studied in details. The mixture of hydrocarbons obtained from hydrothermal treatment of algae biomass is called "oil". Algae *Chlorella sp.* were used as the initial biomass. This type of algae was chosen because *Chlorella sp.* easy to cultivate. The main objective of this research is to study peculiarities of oil and gas production from biomass of algae *Chlorella sp.* using hydrothermal treatment. Experiments on hydrothermal treatment of algae *Chlorella sp.* were carried out. The influence of the mineral phases, the duration of the experiments and the temperature on the yield and composition of the hydrocarbons was determined. Total of 11 experiments were carried out in 2 series: C-3 - with mineral phases, C-7 - experiments of different duration and at different temperatures. All the experiments were carried out in Experimental geochemistry lab of Faculty of geology of MSU. The experiments were carried out at a temperature of 250-350°C and a pressure of saturated water vapor.

All experiments were conducted using 20 ml titanium autoclaves. Aqueous solution and algae tablets were placed in autoclaves. For experiments with mineral phases, algae tablets were used up with minerals in the tulk and were also loaded into autoclaves. Then the autoclaves were closed and placed in the oven for 3 or 7 days. After these days the autoclaves were taken from the oven and either quenched in cold water or gas was taken. To do this, the following actions were performed under water. A funnel was put on the autoclav, and a test tube which the released gas was put on it. The volume of gas was measured with the test tube. Then it was moved to the test tube with brine for storage and examination with a syringe. After it oil was extracted. In some experiments 5 ml of hexane were poured into the autoclave, then using a separating funnel the aqueous solution was separated from the solution of hydrocarbons and hexane and the latter was poured into cans for weighing and evaporation. The

remaining hydrocarbons were extracted from the autoclave with chloroform and were also weighed and evaporated. Then everything was transferred to caddy for storage. In the remaining experiments the contents of the autoclave were poured into a sample bottle, the residue was poured 5 ml of chloroform and also transferred into a sample bottle. Then water solution was taken with a syringe from under a layer of hydrocarbons with chloroform and the residue was evaporated under fume hood, weighed and transferred to caddies for storage. For oil obtained in a series of experiments C-3 and for algae biomass *Chlorella sp.* an isotope analysis of carbon was carried out on the Delta V Advantage complex of light isotope analysis equipment (made in Germany) at the Department of Geology and Geochemistry of Fossil Fuels at Moscow State University.

Based on the results of experiments of the C-3 series, a diagram of dependence of the oil yield on the mineral phase (*Fig. 1*) and histograms of the ratio of maltenes and asphaltenes depending on the mineral phase (*Fig. 2*) were constructed. They also contain data on the output of oil without the mineral phase. Histograms show that the maximum oil yield is in the experiment without the mineral phase, and among the experiments with mineral phases the maximum is found in the experiment with the addition of quartz and calcite the minimum is in the experiment with the addition of aluminum oxide and hematite and montmorillonite have intermediate values of oil output. Minimum of the relative amount of maltenes appears in the experiment without the mineral phase, and the maximum in the experiment with hematite. Realy the ratio of maltenes and asphaltenes in experiments with mineral phases is comparable. It follows that mineral phases accelerate the process of oil ripening. The decrease in oil yield is probably due to the sorption of oil on the surface of the mineral phases. In addition, a diagram of the dependence of $\delta^{13}\text{C}$ on the mineral phases was constructed (*Fig. 3*), the value of $\delta^{13}\text{C}$ of the algal biomass was plotted on it. It shows that both maltenes and asphaltenes are enriched in a light carbon isotope relat ive to the initial biomass. Maltenes to a greater extent. According to the results of a series of experiments C-7, the diagrams of the yield of oil (*Fig. 4*) and gas (*Fig. 5*) depending on the duration of the experiments at different temperatures were constructed. It can be seen from them that the yield of oil increases in the series: $350 > 300 \geq 250^\circ\text{C}$, and gas in the series: $350 > 250 > 300^\circ\text{C}$. With run duration, the amount of oil emissions decreases, while the gas yield increases.

Hydrothermal equilibria and ore formation

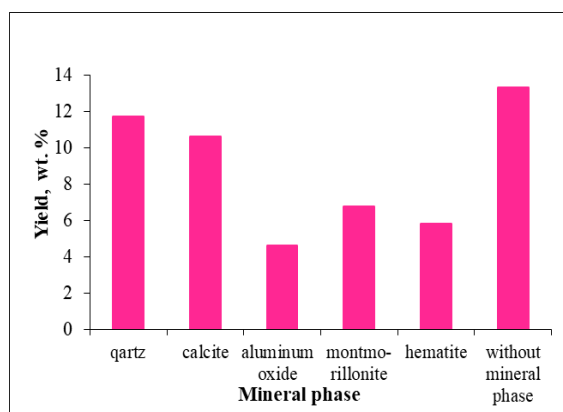


Fig. 1. Chart of oil yield versus mineral phase in a series of experiments C-3.

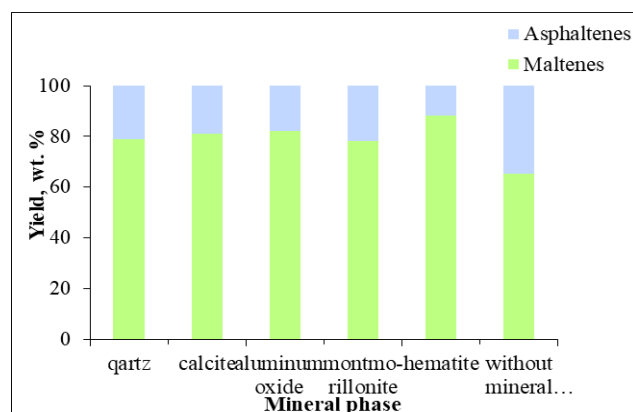


Fig. 2. Histogram of the ratio of maltenes and asphaltenes depending on the mineral phase in a series of experiments C-3.

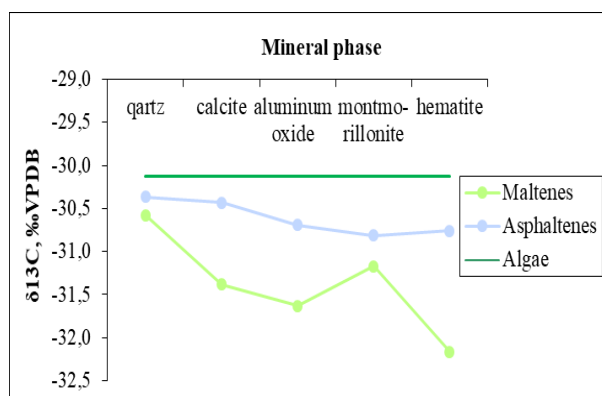


Fig. 3. Carbon isotope fractionation between fractions of maltenes and asphaltenes in the C-3 series of experiments.

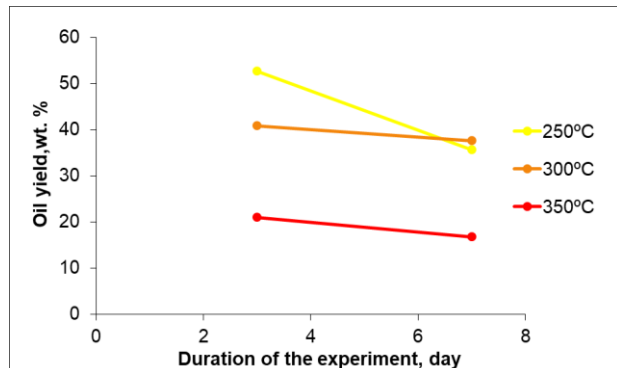


Fig. 4. Oil yield depending on the duration of the experiment at different temperatures.

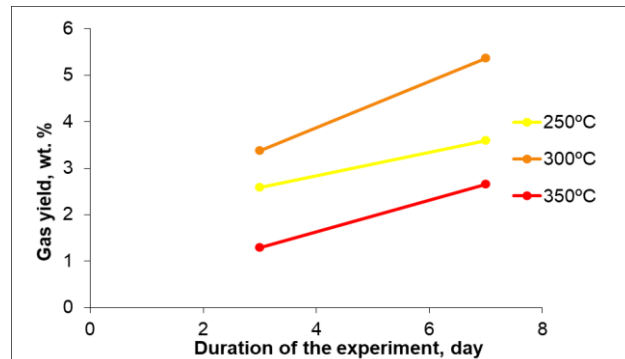


Fig. 5. Gas yield depending on the duration of the experiment at different temperatures.

The following peculiarities of formation of oil from algae were revealed. Mineral phases affect the hydrothermal conversion of algae biomass. The highest yields were obtained in experiments with quartz and calcite, the smallest with aluminum oxide, and intermediate values for hematite and montmorillonite were obtained. The carbon isotope composition showed that both maltenes and asphaltenes are enriched in a light carbon isotope relative to the initial biomass, but maltenes are more. The oil yield increases in the series: 350 > 300 ≥ 250°C, and gas in the series: 350 > 250 > 300°C. With an increase in the duration of the experiments, the

amount of oil output decreases, while that of gas increases.

Acknowledgments: The work was supported by the Russian Foundation for Basic Research, project 18-05-00818.

References:

- Anastasakis K., Ross A.B. Hydrothermal liquefaction of the brown macro-alga *Laminaria Saccharina*: Effect of reaction conditions on product distribution and composition // *Bioresource Technology* 102, 2011, pp. 4876–4883
- Bach Q.-V., Sillero M.V., Tran K.-Q., Skjermo J. Fast hydrothermal liquefaction of a Norwegian macro-

- alga: Screening tests // *Algal Research* 6, 2014, pp. 271–276
- Biswas B., Kumar A.A., Bisht Y., Singh R., Kumar J., Bhaskar T. Effects of temperature and solvent on hydrothermal liquefaction of *Sargassum tenerrimum* algae // *Bioresource Technology* 242, 2017, pp. 344–350
- Chen W.-T., Zhang Y., Zhang J., Yu G., Schideman L.C., Zhang P., Minarick M. Hydrothermal liquefaction of mixed-culture algal biomass from wastewater treatment system into bio-crude oil // *Bioresource Technology* 152, 2014, pp. 130–139
- Chiodo V., Zafarana G., Maisano S., Freni S., Urbani F. Pyrolysis of different biomass: Direct comparison among *Posidonia Oceanica*, *Lacustrine Alga* and *White-Pine* // *Fuel* 164, 2016, pp. 220–227
- Fahmy, T.Y.A., Fahmy, Y., Mobarak, F. et al. Biomass pyrolysis: past, present, and future *Environ Dev Sustain* (2018). <https://doi.org/10.1007/s10668-018-0200-5>
- Shakya R., Whelen J., Adhikari S., Mahadevan R., Neupane S. Effect of temperature and Na₂CO₃ catalyst on hydrothermal liquefaction of algae // *Algal Research* 12, 2015, pp. 80–90
- Shakya R., Whelen J., Adhikari S., Mahadevan R., Neupane S. Effect of temperature and Na₂CO₃ catalyst on hydrothermal liquefaction of algae // *Algal Research* 12, 2015, pp. 80–90
- Reddy H.K., Muppaneni T., Ponnusamy S., Sudasinghe N., Pegallapati A., Selvaratnam T., Seger M., Dungan B., Nirmalakhandan N., Schaub T., Holguin F.O., Lammers P., Voorhies W., Deng S. Temperature effect on hydrothermal liquefaction of *Nannochloropsis gaditana* and *Chlorella* sp. // *Applied Energy* 165, 2016, pp. 943–951
- J. et al. Pyrolysis of algal biomass // *Journal of Analytical and Applied Pyrolysis* 103, 2013, pp. 134–141

Konopleva I.V.¹, Sevast'yanov V.S.¹, Telegina T.A.² Investigation of hydrocarbon biomarkers in bio-oil produced by hydrous pyrolysis of cyanobacteria *Arthrospira platensis* (*Spirulina*) biomass

¹V.I. Vernadsky Institute of Geochemistry and Analytical Chemistry of Russian Academy of Sciences, Moscow, ²Bach Institute of Biochemistry, Research Centre of Biotechnology of Russian Academy of Sciences, Moscow (konopleva@geokhi.ru)

Abstract The work is devoted to the study of the genesis of oil in the Uzon volcano caldera (Kamchatka). The Uzon oil to be believed is largely a product of hydrothermal processing of plant detritus and the biomass of microorganisms that inhabit the caldera thermal waters. The dominant biota are cyano- and chemolithoautotrophic bacteria in the caldera lakes. The objective of the present work was to find a genetic coupling of cyanobacterial organic matter and the Uzon hydrothermal oil. To simulate the process of oil formation, hydrous pyrolysis of the *Arthrospira platensis* (*Spirulina*) dry biomass was carried out at 300°C for 72 h in three environments with various gas composition: (1) Ar + deaerated water, (2) Ar + water, saturated with H₂S, and (3) air + water. The produced bio-

oils were fractionated into saturated + aromatic and polar fractions. The weight ratio of maltenes to asphaltenes in the bio-oils was 1.5:1. The proportion of saturated hydrocarbons was small and ranged from 2 to 3%. The samples of saturated fractions were analysed by gas chromatography (GC), where *n*-alkanes C₂₀-C₃₃ and acyclic isoprenoids were identified. Among *n*-alkanes, *n*-C₁₇ dominated in the bio-oils, its share was in the range from 80 to 87% of the total *n*-alkane content. Isoprenoids phytane, Ph significantly dominated amongst acyclic isoprenoids, its share was 20% of the total alkane content in anaerobic environments (1 and 2), and was 8% in air medium (3). Analysis of the native *Arthrospira platensis* lipid extract revealed predominance of *n*-C₁₇ in the composition of cyanobacterial hydrocarbons as well as in the produced bio-oils. The findings suggest that cyanobacteria could be producers of the hydrothermal Uzon oil.

Keywords: cyanobacteria, hydrous pyrolysis, alkanes, biota, Uzon caldera, Kamchatka

Introduction Oil seeps near hot springs of the hydrothermal fields in the caldera of Uzon volcano (Kamchatka) were discovered. At present, most scientists consider a biogenic origin of the Uzon oil as the most reasonable hypothesis. The formation of the Uzon oil seeps is considered as a process of thermolysis or thermocatalytic processing of plant remains and the biomass of microorganisms that inhabit the caldera thermal lakes (Fursenko et al., 2014; Galimov et al., 2015). There is a hypothesis that the Uzon oil seeps are formed as a result of an intensive transformation of lipids of the living matter, which passes for a very short time under aggressive environmental conditions without immersing to significant depths (Varfolomeev et al., 2011; Maryutina et al., 2013).

The biocenosis of the caldera comprises various microbial communities inhabiting the thermal waters. The dominating microorganisms are thermophilic cyano- and chemolithoautotrophic bacteria (Gumerov et al., 2011). The photo- and chemosynthetic organic matter produced by the autotrophic organisms could be the source of hydrocarbons.

The study of the transformation of bacterial biomass organic matter (OM) as a result of hydrous pyrolysis contributes to the understanding of biogeochemical processes of the hydrothermal oil formation. Essential information on the conversion of microorganisms into oil under hydrotherms can be provided by studying of hydrocarbons formed from the of bacterial biomass as a result of hydrothermal processing.

The objective of the work was the study of hydrocarbon-biomarkers in bio-oil, formed as a result of hydrous pyrolysis of cyanobacteria (blue-green algae), which are likely the producers of the Uzon oil seeps.

Objects and methods of research The object of the study was dry biomass of *Arthrospira platensis*

Hydrothermal equalibria and ore formation

(*Spirulina*) grown in a photobioreactor on Zarruk medium. Hydrous pyrolysis of the *Arthrospira platensis* biomass was carried out in titanium capsules at 300°C for 72 h in three environments: (1) Ar + deaerated water, (2) Ar + water, saturated with H₂S, and (3) air + water. The choice of the environment 2 is due to the presence of dissolved hydrogen sulphide in thermal waters of the caldera, which comes from the depths as part of hydrothermal gases.

After the high-pressure titanium capsules cooled down, they were opened and the pyrolisates were obtained by washing with methanol (MeOH)/chloroform (TCM) (1:1 v/v). After filtration through glass wool, the pyrolisates were poured into separatory funnel for separation of organic and water layers. After 10 ml of *n*-hexane/TCM (2:1 v/v) were added to water layer, the mixture was shaken vigorously for 1 min, the funnel was then allowed to stand for 10 min. The *n*-hexane/TCM organic layer was transferred to vial. The organic extracts were combined, concentrated by evaporation, then poured with excess of *n*-hexane (1:40 v/v) to isolate asphaltenes. To separate maltenes from asphaltenes a glass filter was used. Maltenes were fractionated into saturated + aromatic and polar fractions.

To extract lipids from untransformed (native) cyanobacteria, the *Arthrospira platensis* biomass was filled with TCM/MeOH (2:1 v/v) and left overnight. After mixture was kept in the ultrasonic bath for 30 minutes, the extract was separated from the biomass by decantation and concentrated by evaporation in air. The extract was subjected to fractionation for separation of saturated fraction. The samples of saturated fractions were analysed by gas chromatography. We used GC Perkin-Elmer, Clarus-500 with flame ionization detector (FID) and silica capillary column (30 m x 0.32 mm i.d., 0.25 µm film thickness), and He, as a carrier gas. The oven was programmed from 45°C to 315°C (ramp at 4°C/min), and a final temperature was held for 50 min.

Results and discussion The weight ratio of maltenes to asphaltenes in three bio-oils was similar (1.5:1). Maltenes consist mainly of polar compounds. The proportion of the saturated hydrocarbons (HC) in three bio-oils ranged from 2 to 3% (Fig. 1).

Only short-chain *n*-alkanes C₁₅, C₁₆, C₁₇ were detected in the saturated fraction of the native *Arthrospira platensis* biomass, where the portion of *n*-C₁₇ was 90%.

n-Alkanes C₁₃ - C₃₃ were identified in saturated fractions of the bio-oils. The portion of *n*-C₁₇ was also maximal and ranged from 80 to 87%, the portion of *n*-C₁₅ was within 6-11%, the share of *n*-C₁₆ was in the range from 3 to 5%, the rest was <1% of the total *n*-alkane content.

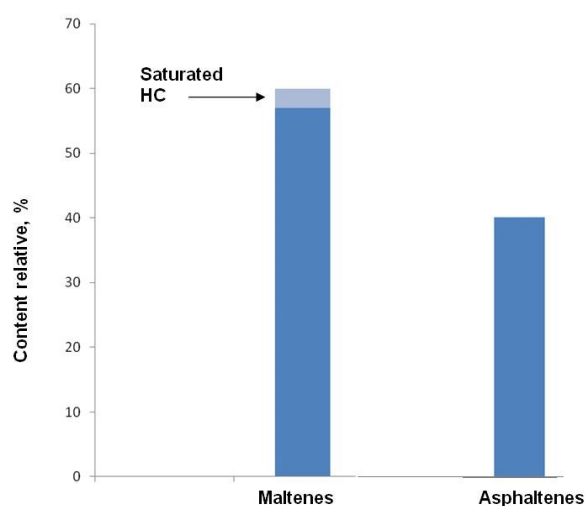


Fig. 1. Diagram of the bio-oil group composition

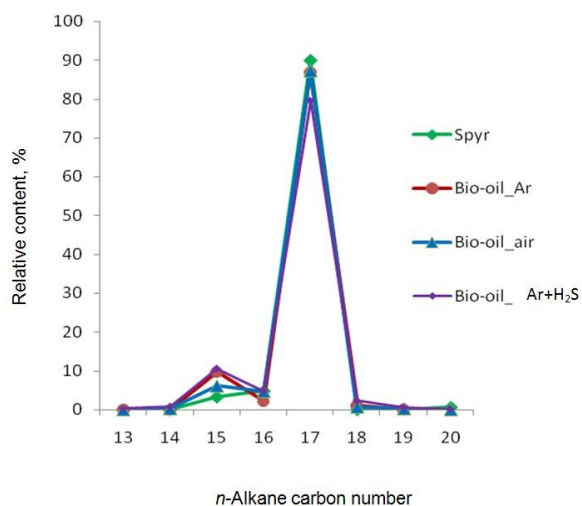


Fig. 2. Molecular-mass distribution of *n*-alkanes in the native and the hydrothermally transformed *Arthrospira platensis*

The distribution of *n*-alkanes in the native *Arthrospira platensis* biomass and the cyanobacterial biomass, subjected to hydrous pyrolysis in the environments with various gas composition, demonstrates that *n*-C₁₇ prevails to a large extent in all samples (Fig. 2). It is known that the majority of carbon chains synthesized by living organisms contain an even number of C atoms and the predominant content of odd alkanes during thermal conversion is usually associated with the processes of fatty acids decarboxylation. However, the experimental data suggest that odd alkane *n*-C₁₇ is a biosynthetic product of *Arthrospira platensis* metabolism and not the result of hydrothermal conversion of substances constituting lipids.

Figure 3 shows an increase of the *n*-C₁₅ content in a row: native biomass → hydrous pyrolysis in air → hydrous pyrolysis in Ar and (Ar + H₂S), which suggests that *n*-C₁₅ is formed in hydrothermal oil as a

result hydrothermal processing of cyanobacterial organic matter under reductive conditions.

Acyclic isoprenoids phytane Ph and pristane Pr were identified in three bio-oils generated in the environments with various gas composition. The source of these hydrocarbons is alcohol phytol, which is a part of cyanobacteria chlorophyll. Pristane is formed by oxidation and decarboxylation of phytol, and phytane is generated as a result of phytol dehydration and reduction. The portion of Ph was about 20% of the total alkane content in environments (1) and (2), and was 8% in environment (3). The ratio Pr/Ph = 0.06 in oxygen free environments (1) and (2), and Pr/Ph = 0.10 in air environment (3).

Unlike the bio-oils, Pr was not found, and the portion of Ph was insignificant (about 1% of the total alkane content) in the native *Arthrospira platensis* biomass.

In 2014, the sample of biota was collected from the water surface of thermal lake, which is situated within the bounds of the Central hydrothermal field of the Uzon caldera. The sample consisted of organic and mineral matter. It was decarbonatized, rinsed, and dried. The soluble part of the biota, extracted by benzene/MeOH (9:1 v/v.), was subjected to fractionation for isolation a fraction of saturated hydrocarbons. The composition of *n*-alkanes was determined. Figure 3 shows the relative content of *n*-alkanes in the biota, converted under hydrotherms (in the temperature range of 40-100 ° C), and in the native *Arthrospira platensis* biomass.

It can be seen that *n*-C₁₇ dominates in *n*-alkane composition of both samples. In our previous work (Konopleva et al., 2017), the genetic relationship of biota with the Uzon oil has been established. These findings suggest that cyanobacteria could be producers of the Uzon caldera oil seeps.

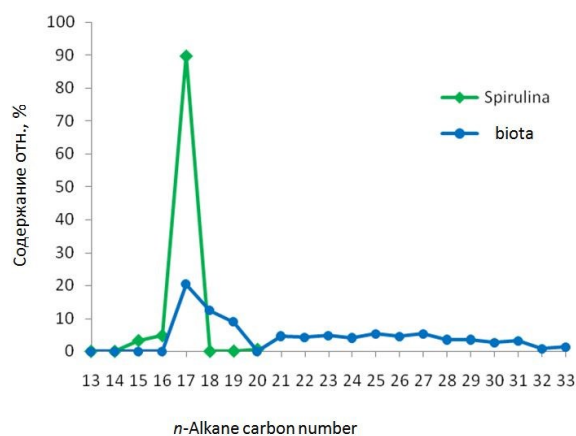


Fig. 3. The distribution of *n*-alkanes in the biota (the Uzon caldera) and in the native *Arthrospira platensis* biomass

Conclusion Alkanes of normal and isoprenoid structure were found in the bio-oils produced as a result of hydrous pyrolysis of the *Arthrospira*

platensis biomass in the environments with various gas composition. Among *n*-alkanes, *n*-C₁₇ dominated in three bio-oils, its share ranged from 80 to 87% of the total *n*-alkane content. Among isoprenoids, Ph significantly dominated in the bio-oils, its share was about 20% of the total alkane content in oxygen free environments (Ar + deaerated water, Ar + water, H₂S) and was 8% in air environment (3). No significant differences were found in the hydrocarbon composition of the bio-oils formed in inert (1) and reductive (2) environments.

n-Alkanes C₁₅-C₂₀ have been identified in the *Arthrospira platensis* lipid extracts. Among *n*-alkanes, *n*-C₁₇ dominated, its share was about 90% of the total *n*-alkane content.

The results revealed that *n*-C₁₇ was a product of bacterial synthesis and not the result of hydrothermal conversion of substances constituting lipids.

Among *n*-alkanes, *n*-C₁₇ dominated in the biota collected in the thermal lake of the Uzon caldera as well as in the native *Arthrospira platensis* biomass and in the produced three bio-oils.

The findings suggest that cyanobacteria could be a producer of hydrothermal oil from the Uzon caldera.

References:

- Varfolomeev S. D., Karpov G. A., Sinal, G. A., Lomakin S. M., Nikolaev E. N. The Youngest Natural Oil on Earth. Doklady Chemistry, 2011, Vol. 438, Part. 1, pp. 144-147, doi: 10.1134/S0012500811050053
- Galimov, E. M., Sevast'yanov, V. S., Karpov G. A., Kamaleeva A.I., Kuznetsova O.V., Konopleva I.V., Vlasova L.N. Hydrocarbons from a Volcanic Area. Oil seeps in the Uzon caldera, Kamchatka. Geochem. Int., 2015, Vol. 53, pp. 1019-1027, doi:10.1134/S0016702915120046
- Gumerov V.M., Mardanov A.V., Beletsky A.V., Bonch-Osmolovskaya E. A., Ravin N. V. Molecular analysis of microbial diversity of microorganisms in the Zavarzin Spring, Uzon Caldera, Kamchatka. Microbiology, 2011, V. 80, No.2, 244-251, doi: 10.1134/S002626171102007X
- Konopleva I.V., Sevast'yanov V.S., Kuznetsova O.V., Vlasova L.N., Galimov E.M. Experimental modeling of biota's organic matter catagenetic transformation. Relationship with oil genesis. //Experiment in Geosciences, 2017, V. 23, No. 1, p.p. 149-152. <http://www.iem.ac.ru>
- Maryutina T.A., Karpov G.A., Varfolomeev S.D. Basic Hydrocarbon Components and Chemical Composition of the Environmental Medium of the Youngest Oil on Earth. Doklady Chemistry, 2013, Vol. 449, Part. 1, pp. 77-80, doi: 10.1134/S0012500813030026
- Fursenko E. A., Kashirtsev V. A., Kontorovich A. E., Fomin A. N. Naphthides of continental hydrotherms (Uzon, Yellowstone, New Zealand): Geochemistry and genesis. Russian Geology and Geophysics, 2014, Vol. 55, No. 5-6, pp. 726-736, doi:10.1016/j.rgg.2014.05.015

Hydrothermal equilibria and ore formation

Kotova N.P. Experimental study of temperature influence on niobium oxide solubility in chloride NaCl and LiCl solutions.

Institute of Experimental Mineralogy RAS, Chernogolovka, Moscow district (kotova@iem.ac.ru)

Abstract. The dependence of Nb₂O₅ solubility as a function of temperature was investigated in NaCl and LiCl solutions with concentrations 0.1 and 1 m at 300 - 550 °C and 100 MPa under Co-CoO oxidizing conditions. It was found that in chloride solutions of different cationic composition (NaCl and LiCl), the temperature dependence of the solubility of Nb₂O₅ in the temperature range of 300-550 °C and P = 100 MPa, (Co-CoO buffer) is weakly expressed. The solubility of Nb₂O₅ is low and remains in the range of 10⁻⁵ m.

Keywords: experiment, oxide niobium, hydrothermal solubility, temperature, chloride solutions

At present, the most common point of view on the processes leading to Nb – Ta mineralization is the model of high-temperature metasomatism, according to which the crystallization of granite magma in the residual melt is the accumulation of Li, Nb, Ta and F, which in turn, with further cooling form a small accessory impregnation of Nb – and Ta – containing minerals. However, along with magmatic processes, hydrothermal transport of these elements undoubtedly plays an important role. Quantitative description of transport and deposition processes by Nb and Ta hydrothermal fluids requires knowledge of the forms of finding of these elements in the fluids. Currently, this kind of information is sketchy or completely absent. Therefore, we are carried out systematic experimental studies on the solubility of rare metals in a wide range of temperatures and pressures corresponding to the physical and chemical parameters of postmagmatic processes.

New experimental data on the solubility of niobium oxide (Nb₂O₅), an analog of the natural

mineral nioboxide, were obtained in aqueous chloride solutions consisting of 0.1 and 1.0 m NaCl and LiCl at 400 and 500 °C and 100 MPa under Co-CoO oxidizing conditions. The run duration was 21 days. Experiments were performed on a hydrothermal line. A sealed-capsule quench technique was employed. The same technique was used to study Ta₂O₅ and Nb₂O₅ solubility in fluoride solutions.

The quenched aqueous solutions were then analyzed using ICP/MS (Inductively Coupled Plasma Mass Spectrometry) and ICP/AES (Atomic Emission Spectroscopy) for Nb, Ta, Mn, and Fe and admixture elements Ti, W, and Sn.

To control congruent or incongruent dissolution of Nb oxide and to determine chemical composition of newly-formed phases (in case of their detection) the initial materials and solid run products were studied by X-ray diffraction, and electron microprobe analysis (Cam Scan MV 2300 (VEGA TS5130MM)).

Experimental data on the solubility of Nb₂O₅ in 0.1 and 1m NaCl solutions at 300-550 °C and P = 100 MPa as a function of temperature are shown in Fig. 1. Studies have shown that in NaCl solutions at all studied temperatures the equilibrium content of niobium is low and practically does not depend on the concentration of sodium chloride. With an increase in temperature from 300 to 550 °C, the equilibrium content of niobium in solutions of 0.1 and 1 m NaCl practically does not change, remaining at the level of 10⁻⁵ mol/kg H₂O. Studies have shown that in solutions of NaCl at all temperatures considered, the equilibrium content of niobium is low and practically does not depend on the concentration of sodium chloride. As the temperature rises from 300 °C to 550 °C, the content of niobium in solutions of 0.1 and 1 m NaCl remains in the range of 10⁻⁵ mol/ kg H₂O (Fig. 1).

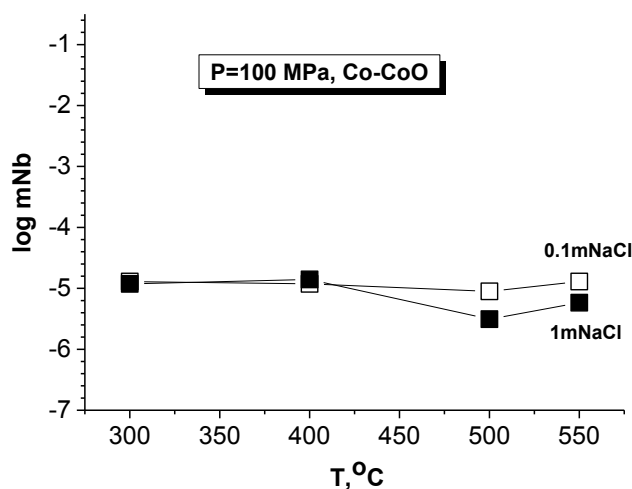


Fig. 1. Temperature dependence of Nb₂O₅ solubility in NaCl solutions at P = 100 MPa (Co-CoO buffer)

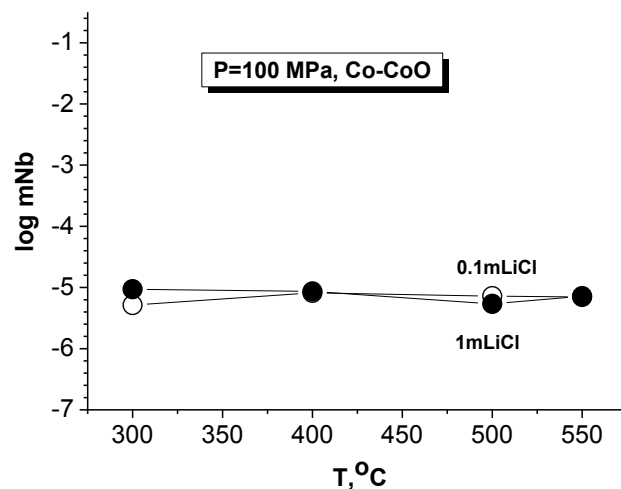


Fig. 2. Temperature dependence of Nb₂O₅ solubility in LiCl solutions at P = 100 MPa (Co-CoO buffer)

Figure 2 shows the temperature dependence trends of niobium oxide solubility in 0, 1 and 1m LiCl solutions at P = 100 MPa. Analysis of the results of experiments on the solubility of niobium oxide in solutions of 0.1 and 1m LiCl showed that the trends of the dependence of the solubility of niobium oxide on temperature are identical. With an increase in temperature from 300 to 550 °C, the equilibrium content of niobium in solutions of 0.1 and 1 m LiCl practically does not change, remaining at the level of 10⁻⁵ mol / kg H₂O. Figures 1 and 2 show that the new experimental results are in good agreement with the previously obtained experimental data on the solubility of niobium oxide in NaCl and LiCl solutions at temperatures of 300 and 550°C and 100 MPa (Kotova; 2015, 2018).

The data of X-ray diffraction of solid run products clearly show that, for the range of concentration of NaCl and LiCl solutions and temperatures considered in this study, at P = 100 MPa, niobium oxide dissolves congruently, that is, without changing its composition. The exception is the data on the solubility of niobium oxide in 1 m LiCl solution at T=550° C and P=100 MPa, where Nb₂O₅ dissolves incongruently. In this case, niobium oxide is partially replaced by lithium niobate LiNb₃O₈.

Experimental studies have suggested that hydrothermal NaCl and LiCl fluids are not able to transport significant quantities of Nb. Transport of large quantities of Nb can only occur in concentrated F – rich solutions.

This work was supported by the grants of RFBR 18-05-01001-a

References:

- Kotova N.P. Experimental study of Nb₂O₅ solubility in chloride solutions at 300-550°C and 100 MPa. Experiment in GeoSciences. 2015. V. 21. N1. P. 41.
 Kotova N.P. Experimental study of temperature influence on niobium oxide solubility in chloride HCl and KCl solutions. Experiment in GeoSciences. 2018. V. 24. N1. P. 143-144

Suvorova V.A.¹, Osadchii V.O.^{1,2}, Akinfiev N.N.^{3,4} The solubility of cassiterite in the SnO₂-H₂O system at 400°C and 260-450 bar. UDC 550.4.02

¹ IEM RAS, Chernogolovka, Moscow Region, Russia (lera@iem.ac.ru), ² MSU, Faculty of Geology, Moscow, Russia (v.osadchii@iem.ac.ru), ³ IGEM RAS, Moscow, Russia (akinfiev@igem.ru), ⁴ MSGPI-RSGPU, Moscow, Russia

Abstract We measured the solubility of cassiterite in low-density water fluid at 400°C and 260-450 bar. Measured solubility is in consistent with cassiterite solubility predicted by Akinfiev-Diamond equation of state for Sn(OH)₄(aq)

with parameters obtained from high-density fluid experiments published elsewhere.

Keywords: cassiterite, tin oxide, solubility, fluid

Tin is a component of many hydrothermal systems, in which, depending on the conditions, it can be in the II and IV-valence state. In natural waters tin is present mainly as hydroxocomplexes, and in HCl-containing waters chlorine ions can act as ligands (Migdisov, Williams-Jones, 2005). Tin exhibits amphoteric properties and neutral complexes SN(OH)₂ and Sn(OH)₄ (Sorokin, Dadze, 1994; Cigala et al.) dominate in a wide pH range., 2012). While the behavior of Sn(II) in hydrothermal systems has been studied quite well (Cigale et al., 2012), the behavior of Sn(IV) was poorly studied due to the low solubility of cassiterite (SnO₂) (Sorokin, Dadze, 1994). The aim of this work was to determine the solubility of Sn(IV) in a low-density supercritical fluid at 400°C and a pressure of 260-450 bar. These data are of interest both for tin Geochemistry and for modelling the disposal of radioactive waste, one component of which is 126Sn (T_{1/2} = 105 years) (Cigala et al., 2012). Solubility experiments were carried out in a titanium (BT 8) autoclave (120 cm³) with an internal ampoule (13 cm³) for in situ vapor phase sampling (Fig. 1) (Zakirov et al., 2007; Akinfiev, Zotov, 2016). The temperature was controlled by S-type thermocouple, pressure – by D100 pressure sensor. The measurement accuracy was =0.3 MPa and 2K, respectively. The experiments used distilled water and crystalline tin oxide SnO₂ produced by Sigma-Aldrich, which was taken with excess. After heating the unit during the day and exposure at a given temperature for 2-3 days (which was enough to establish equilibrium), the internal ampoule was opened for 5 minutes and filled with fluid. After that, the ampoule was closed, and the autoclave was quenched in cold water. Subsequently, the ampoule was washed 5 times with a known amount of Royal vodka. These solutions were diluted 5 times and analyzed by the ISP-MS method.

Table 1. The solubility of cassiterite in water at 400 °C and the corresponding values of log K^o(1)

	P (bar)	$m_{\text{Sn}} \cdot 10^{-6}$ ((mol·kg H ₂ O ⁻¹))	log K ^o
	252.4	0.3	-6.54
	262.1	8.1	-5.09
	266.4	12.4	-4.91
	263.7	0.3	-6.55
	272.8	0.4	-6.41
	275.1	1.0	-6.01
	275.3	9.9	-5.00
	248.3	2.5	-5.61
			-5.76
<i>Average</i>	264.5 ± 7.0*	4.4 ± 3.4	± 0.49
	291.7	0.2	-6.77

Hydrothermal equilibria and ore formation

	P (bar)	$m_{\text{Sn}} \cdot 10^{-6}$ ((mol·kg H ₂ O ⁻¹))	$\log K^\circ$
	291.5	0.2	-6.61
	288.5	2.5	-5.61
	294.9	1.9	-5.73
	293.3	0.7	-6.18
<i>Average</i>	291.98 ±2.1	1.1 ±0.9	±0.45
			-5.62
	449.5	2.4±3.4**	±0.49**

* Confidence interval 95%

**The confidence interval for the unit value was taken from experiments at 248-275 bar

The solubility values measured at close P-T parameters were averaged, resulting in the solubility of SnO₂ at a pressure of 264, 293 and 450 bar (Table. 1).

Processing of experimental data (Sorokin, Dadze, 1994) on the solubility of cassiterite at temperatures of 200 – 400°C and P_{SAT} – 150 MPa, as well as the description of the thermodynamic properties of Sn(OH)₄(aq) were based on the Akinfiev- Diamond equation of state (Akinfiev, Diamond, 2003). (Figure 2).

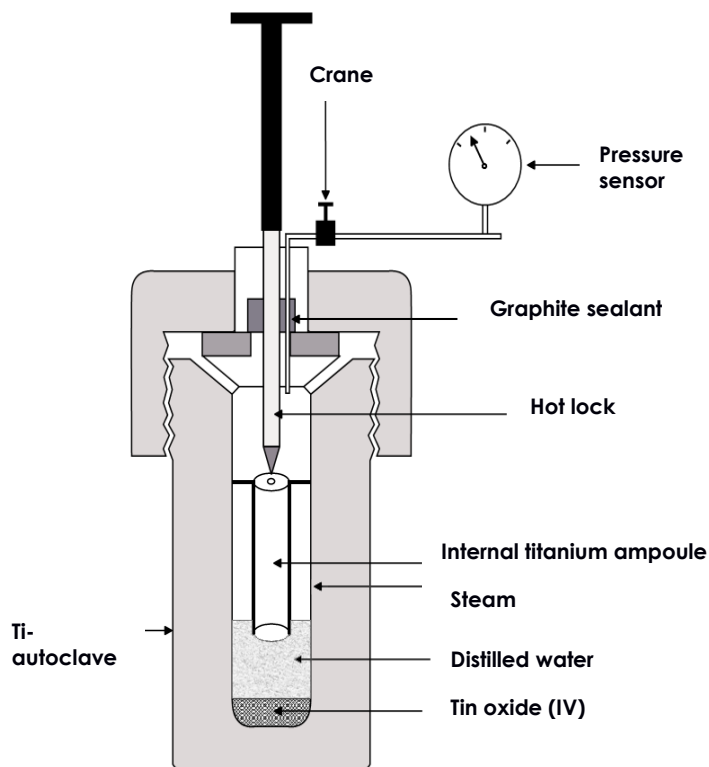


Figure 1. Scheme of the titanium autoclave with an internal amp, allowing the sample *in situ*.

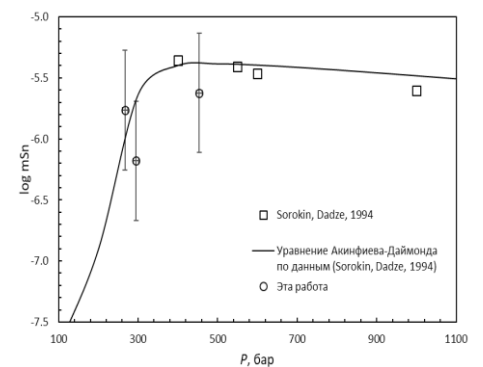
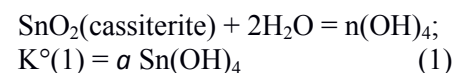


Figure 2. Solubility of tin in aqueous fluid at 400°C and different pressure.

The reaction of dissolution of cassiterite can be written in the form:



This equation was originally used to describe neutral molecules of volatile components in an infinite dilution state over a wide range of temperatures (0-800°C) and pressures (0.1–300 MPa), and then generalized to the case of non-volatile hydroxides (Si(OH)₄(aq), Ge(OH)₄(aq)) (Akinfiev, Plyasunov, 2014).

In this model, the standard chemical potential of the dissolved component at a given temperature T (K) and pressure P (MPa) is written as)

$$\mu_{2,aq}^\infty(P, T) = \mu_{2,g}^\circ(T) - RT \ln N_w + (1 - \xi)RT \ln \frac{f_1^*}{P^\circ} + RT \xi \ln \left(\frac{RT}{P^\circ M_w} \rho_1^* \right) + RT \rho_1^* \left[a + b \left(\frac{10^3}{T} \right)^{0.5} \right],$$

where $\mu(\text{SnO}_2(\text{cr.}))$ и μ_1^* – chemical potentials of cassiterite and water at a given temperature T and pressure P , and a m – the experimental value of solubility in mol/kg.

Table 2. Thermodynamic properties of the gas molecule Sn(OH)₄

Component	Properties of a molecule in the ideal gas state			Akinfiev-Diamond equation Parameters of the of state		
	$\Delta_f G^\circ_{298}, \text{kJ} \cdot \text{mol}^{-1}$	$S^\circ_{298}, \text{J} \cdot \text{mol}^{-1} \cdot \text{K}^{-1}$	$C_p(T), \text{J} \cdot \text{mol}^{-1} \cdot \text{K}$	ξ	$a, \text{cm}^3 \cdot \text{g}^{-1}$	$b, \text{cm}^3 \cdot \text{K}^{0.5} \cdot \text{g}^{-1}$
Sn(OH) ₄	-841.7 ± 6.1	380.2	$140.14 + 59.84 \cdot 10^{-3} \cdot T - 207 \cdot 10^6 \cdot T^{-2} - 3.499 \cdot 10^{-5} \cdot T^2 + 9.916 \cdot 10^{-9} \cdot T^3$	-3.404 ± 0.30	19.66 ± 3.5	-13.03 ± 2.3

The obtained values of the thermodynamic properties of Sn(OH)₄ are presented in Table 2.

The solubility of cassiterite in a low-density aqueous fluid, calculated using the thermodynamic properties of Sn(OH)₄ (aq) and the Akinfiev-Diamond equation of state, is consistent with the results of the experiment. The thermodynamic parameters of the gas particle Sn(OH)₄ (aq) given in this paper can be used with caution when modeling hydrothermal processes involving tin. Additional experiments on the solubility of tin in the supercritical fluid at temperatures other than 400°C, as well as in the vapor phase at P_{sat}, will provide a more reliable thermodynamic description of Sn(OH)₄ (aq).

We are grateful to Ya.V. Bychkova for conducting ICP-MS analysis.

References:

- Akinfiev NN, Diamond LW (2003) Thermodynamic description of aqueous nonelectrolytes at infinite dilution over a wide range of state parameters. *Geochim Cosmochim Acta* 67:613–627. doi: 10.1016/S0016-7037(02)01141-9
- Akinfiev NN, Plyasunov AV (2014) Application of the Akinfiev-Diamond equation of state to neutral hydroxides of metalloids (B(OH)₃, Si(OH)₄, As(OH)₃) at infinite dilution in water over a wide range of the state parameters. *Geochim. Cosmochim Acta* 126:338–351. doi: 10.1016/j.gca.2013.11.013
- Akinfiev NN, Zotov AV. (2016) Solubility of chlorargyrite (AgCl(cr./l.)) in water: New experimental data and a predictive model valid for a wide range of temperatures (273–873K) and water densities (0.01–1 g·cm⁻³). *Geochim Cosmochim Acta* 178:178–194. doi: 10.1016/j.gca.2016.01.027
- Cigala RM, Crea F, De Stefano C, et al (2012) The inorganic speciation of tin(II) in aqueous solution. *Geochim Cosmochim Acta* 87:1–20. doi: 10.1016/j.gca.2012.03.029
- Frisch M.J., Trucks G.W.... Fox. D.J. (2009) Gaussian 09, Revision C.01, Gaussian, Inc., Wallingford CT.
- Migdisov AA, Williams-Jones AE (2005) An experimental study of cassiterite solubility in HCl-bearing water vapour at temperatures up to 350 °C. Implications for tin ore formation. *Chem Geol* 217:29–40. doi: 10.1016/j.chemgeo.2004.11.018
- Plyasunov AV., O'Connell JP., Wood RH (2000) Infinite dilution partial molar properties of aqueous solutions of nonelectrolytes. I. Equations for partial molar volumes at infinite dilution and standard thermodynamic functions of hydration of volatile nonelectrolytes over wide ranges of conditions. *Geochim. Cosmochim. Acta* 64: 495-512. Doi: [https://doi.org/10.1016/s0016-7037\(99\)00322-1](https://doi.org/10.1016/s0016-7037(99)00322-1)
- Sorokin VI, Dadze TP (1994) Solubility and complex formation in the systems Hg-H₂O, S-H₂O, SiO₂-H₂O and SnO₂-H₂O. In: *Fluids in the Crust*. Springer Netherlands, Dordrecht, pp 57–93
- Zakirov IV, Sretenskaja NG, Aranovich LY, Volchenkova VA (2007) Solubility of NaCl in CO₂ at high pressure and temperature: First experimental measurements. *Geochim Cosmochim Acta* 71:4251–4255. doi: 10.1016/j.gca.2007.01.028